Estimation of intravoxel incoherent motion (IVIM) parameters in vertebral bone marrow: a comparative study of five algorithms

Jie Liu, Ahmad Karfoul, Louis Marage, Huazhong Shu, Giulio Gambarota

Estimation of intravoxel incoherent motion (IVIM) parameters in vertebral bone marrow: a comparative study of five algorithms

Jie Liu[1,2,3*], Ahmad Karfoul[3,4], Louis Marage[5], Huazhong Shu[1,3] and Giulio Gambarota[3,4]

[1*]Laboratory of Image Science and Technology (LIST), School of Computer Science and Engineering, Southeast University, Nanjing 210096, China.
[2]College of Information Science and Technology, Nanjing Forestry University, Nanjing 210037, China.
[3]Univ Rennes, Southeast University, INSERM, Centre de Recherche en Information Biomèdicale sino-français (CRIBs)-LIA, F-35000 Rennes, France.
[4]Univ Rennes, INSERM, LTSI-UMR 1099, F-35000 RennesFrance.
[5]Department of Medical Physics, Georges François Leclerc Cancer Center, F-21000 Dijon, France.

*Corresponding author(s). E-mail(s): liujie.list@seu.edu.cn;

Abstract

Objective: To access the performances of different algorithms for quantification of IntraVoxel Incoherent Motion (IVIM) parameters $\boldsymbol{D}$, $\boldsymbol{f}$, $\boldsymbol{D^*}$ in Vertebral Bone Marrow (VBM).
Materials and Methods: Five algorithms were studied: four deterministic algorithms (the One-Step and three segmented methods: Two-Step, Three-Step, and Fixed-$\boldsymbol{D^*}$ algorithm) based on the least-squares (LSQ) method and a Bayesian probabilistic algorithm. Numerical simulations and quantification of IVIM parameters $\boldsymbol{D}$, $\boldsymbol{f}$, $\boldsymbol{D^*}$ in vivo in vertebral bone marrow, were done on six healthy volunteers. The One-way repeated-measures analysis of variance (ANOVA) followed by Bonferroni's multiple comparison test (p-value = 0.05) was applied.
Results: In numerical simulations the Bayesian algorithm provided the best estimation of $\boldsymbol{D}$, $\boldsymbol{f}$, $\boldsymbol{D^*}$ compared to the deterministic algorithms. In vivo VBM-IVIM, the values of $\boldsymbol{D}$ and $\boldsymbol{f}$ estimated by the Bayesian algorithm were close to those of the One-Step method, in contrast to the three segmented methods.
Discussion: The comparison of the five algorithms indicates that the Bayesian algorithm provides the best estimation of VBM-IVIM parameters, in both numerical simulations and in vivo data.

Keywords: Bone Marrow, MRI, IntraVoxel Incoherent Motion, least squares, Bayesian inference

1 Introduction

In recent years there has been an increased interest for Intravoxel Incoherent Motion MRI [1] in Vertebral Bone Marrow (VBM-IVIM), for quantification of the diffusion coefficient D, the perfusion fraction f and the pseudo-diffusion coefficient D^*. A first attempt of VBM-IVIM measurements was performed by Yeung et al. [2] in 2004; however, only the diffusion coefficient D was evaluated, since the bi-exponential analysis of the IVIM diffusion decay could not yield a reliable estimation of f and D^*.

In 2014, Marchand et al. showed the feasibility of measuring the IVIM parameters D, f, and D^* in vertebral bone marrow of young, healthy volunteers [3]. Improvements in MRI hardware and MRI sequences, as well as the optimization of acquisition parameters such as the b-values, certainly contributed to the noteworthy quantification of D, f, and D^*. Between 2015 and 2020, VBM-IVIM MRI has been successfully applied in a number of studies, with a major focus on oncology [4–12].

Further developments in VBM-IVIM data acquisition have been recently presented by Lasbleiz et al [13]. First, it was shown that an improved image quality, in terms of better spatial resolution and reduced susceptibility artifacts, could be obtained by employing a multi-shot readout-segmented EPI (RESOLVE [14], readout segmentation of long variable echo train) instead of the single-shot EPI, which had been used in all previous VBM-IVIM studies. Secondly, the SPAIR (Spectrally Adiabatic Inversion Recovery) technique was used for fat saturation, yielding VBM-IVIM images with an increased signal-to-noise ratio (SNR) when compared to the STIR (Short TI Inversion Recovery) technique [13].

The advances in VBM-IVIM data acquisition have not been followed by similar developments in VBM-IVIM data analysis methods, to date. This is in contrast with the IVIM investigations of other organs/tissues (liver, pancreas, etc.), where dedicated analyses of different IVIM quantification strategies have been conducted [15–20].

The aim of the current study was to investigate the performances of different algorithms for the quantification of D, f, and D^* in vertebral bone marrow. Five algorithms were considered: four deterministic least-squares (LSQ) based algorithms (the One-Step, Two-Step, Three-Step, and Fixed-D^* algorithm) and a probabilistic algorithm based on the Bayesian Probability Inference [21]. The performances of each algorithm were evaluated by numerical simulations and tested on VBM-IVIM data acquired in young healthy volunteers at 1.5T.

2 Materials and Methods

2.1 MR Imaging

All experiments were conducted in accordance with the procedures approved by the local Institutional Review Board. Written informed consent was signed by each volunteer before the measurements. MRI data were acquired on a 1.5T MAGNETOM Aera system (Siemens Healthcare, Erlangen, Germany) using spine and body receiver coils. After anatomical T1-weighted and T2-weighted MRI acquisitions, VBM-IVIM measurements were carried out on the lumbar spine of six healthy, young volunteers (age range 18-29 years, mean age 26.1±4.0 years, three women and three men). VBM-IVIM MRI was performed in sagittal orientation using the RESOLVE sequence, with the parameters proposed by Lasbleiz et al. [13]; here briefly: repetition time 2400 ms, echo time 58 ms, field of view (FOV) 400 × 400 mm^2, matrix size 188 × 188, slice thickness 6 mm (10 slices), seven b-values of 0,50,100,150,400,800,1000 s/mm^2, iPAT 3, and the Spectral Attenuated Inversion Recovery (SPAIR) fat saturation. Two repeated, identical RESOLVE acquisitions were performed on five volunteers. The tissue SNR achieved with the current experimental set-up was then calculated using the dual acquisition, subtraction method [22] on the image at $b = 0\ s/mm^2$. To

2.2 Data fitting algorithms

To estimate the IVIM parameters D, f, and D^*, a bi-exponential model was fitted to the IVIM signal intensity for each voxel:

$$S_b = S_0\left(fe^{-bD^*} + (1-f)e^{-bD}\right) \qquad (1)$$

where S_0 is the signal intensity at $b = 0\ s/mm^2$, D, f and D^* are the diffusion coefficient, perfusion fraction and pseudo-diffusion coefficient, respectively. The values of the IVIM parameters

were computed using i) four deterministic algorithms (the One-Step, Two-Step, Three-Step, and Fixed-D^* algorithm) where model parameters are computed in an LSQ way and ii) a probabilistic algorithm where those parameters are obtained by inferring their posterior probability distribution function (PDF).

- *One-Step algorithm*

The estimation of the IVIM parameters was done by fitting the data directly to the equation (1), in a single step using the MATLAB fit function with the Trust Region (TR) algorithm [23] as optimizer. Thus, in the One-Step algorithm the values of the IVIM parameters are simultaneously determined.

- *Two-Step algorithm*

The Two-Step and Three-Step algorithms are an example of segmented strategies, where parameters are estimated separately in different steps [24]. Segmented approaches have been previously proposed for quantification of IVIM parameters; in general, these strategies are more robust to noise and therefore are of interest for data characterized by a low SNR. In the Two-Step algorithm the diffusion coefficient D was estimated by a mono-exponential function, using only the data where the perfusion component could be neglected ($b \geq 200\ s/mm^2$). Once the diffusion coefficient D was obtained, it was fixed to its estimated value and the parameters f and D^* were then estimated by fitting the data to the equation (1) in LSQ way using the TR algorithm.

- *Three-Step algorithm*

As in the Two-Step algorithm, an estimate of D was obtained by using a mono-exponential fitting of data corresponding to b-values greater than $200\ s/mm^2$. The same mono-exponential analysis provided also S_{mono}, which is the value of the estimated signal at the b-value of $0\ s/mm^2$. Then, the perfusion fraction f was obtained from the following formula [25]:

$$f = 1 - \frac{S_{mono}}{S_0} \tag{2}$$

In the last third step, with parameters D and f being fixed to their estimates, the parameter D^* was determined by fitting data at all b-values to the equation (1) also in an LSQ way using the TR algorithm.

- *Fixed-D^* algorithm*

This algorithm relies on specifying a priori the parameter D^* [26]. In this study, D^* was fixed to $(15 \times 10^{-3}\ mm^2/s)$, a value obtained from previous studies [13]. The estimation of D and f was obtained by fitting the data to the equation (1), with the TR algorithm.

- *Bayesian-based algorithm*

In addition to the commonly used non-linear LSQ algorithms, there has been an increasing interest in the Bayesian-based fitting algorithm within IVIM framework [27–29]. This algorithm is based on Bayesian probability inference. The definition of Bayes' theorem for a bi-exponential IVIM model can be written as:

$$P(\theta|S,I) = \frac{P(\theta|I)P(S|\theta,I)}{P(S|I)} \tag{3}$$

where $S \equiv \{S_b\}_{\forall b}$ is the set of signal intensity of one voxel, acquired over all b-values, $\theta = \{S_0, f, D, D^*\}$ denotes the set of all model parameters and I stands for the prior information. $P(\theta|S,I)$, $P(S|\theta,I)$ and $P(\theta|I)$ are the parameters posterior PDF, the data likelihood PDF and the parameters prior PDF, respectively. It should be noted that $P(S|I)$, the direct PDF of the data, is a normalization factor that can be dropped from the following calculation. A bounded Gaussian distribution is employed as a prior distribution for each IVIM parameter in θ [30].To be more specific, the prior probability $P(\nu|I)$, $l_\nu \leq \nu \in \theta \leq h_\nu$, follows a Gaussian distribution $\mathcal{N}(\mu_\nu, \sigma_\nu)$ of a mean, μ_ν, and a standard deviation, σ_ν where l_ν and h_ν are denoting the lower and higher bounds of the parameter $\nu \in \theta$. Let $Q = \sum_b \left(S_b - S_0(fe^{-bD^*} + (1-f)e^{-bD})\right)^2$ be the data fidelity term and M is the number of b-values. Then the likelihood $P(S|\theta,I)$ of the data given the prior information and model parameters is of the form:

$$P(S|\theta,I) \propto (\frac{Q}{2})^{-M/2} \tag{4}$$

It should be noted that the equation (4) is the result of a marginalization of the noise [31]. Then,

Table 1: **Parameter settings for Metropolis Hastings sampling method**

ν	normalized S_0	$f(\%)$	$D(\times 10^{-3}\ mm^2/s)$	$D^*(\times 10^{-3}\ mm^2/s)$
Initial guess of μ_ν	1.0	10	0.5	15
Lower bound l_ν	0.5	1	0.001	5
Higher bound h_ν	1.5	40	2	50

The set of parameters characterizing the prior distribution $P(\nu|I) = \mathcal{N}(\mu_\nu, \sigma_\nu)$, $\nu \in \theta\{f, D, D^*\}$ with $\sigma_\nu = (h_\nu - l_\nu)/3$

under the assumption of the statistical independence of the model parameters, the parameters posterior PDF can be written as follows:

$$P(\theta|S, I) \propto P(f|I)P(D|I)P(D^*|I)(\frac{Q}{2})^{-M/2} \quad (5)$$

A Monte Carlo Markov Chain (MCMC) approach was then employed to calculate the expectations of the IVIM parameters [21, 32], and the Metropolis-Hastings (MH) Sampling method [33] was used to iteratively generate the Markov Chain. For each voxel, the parameters' expectations were calculated from 50000 MCMC samples (50 simulations sampled 1000 times each). In this study, the burn-in number for each Markov chain was set to 50, and a simple mean of the marginal posterior distributions was used [27, 29]. At each iteration of this procedure, the mean $\mu_\nu, \forall \nu \in \theta$, is updated while the standard deviation, σ_ν, is kept fixed to a value equal to $(h_\nu - l_\nu)/3$. An initial guess of μ_ν, is set according to Table 1 obtained from previous studies [4, 13].

2.3 Numerical simulations

Numerical simulations were performed to explore the performances of the five different algorithms for the estimation of the IVIM parameters. Two simulated experiments were designed: in the first experiment, a single set of tissue parameters D, f and D^* was taken as ground truth; in the second experiment, a range of tissue values of D, f and D^* was investigated.

In **the first experiment**, the following parameters were used to generate a noise-free IVIM signal: 1) with respect to tissue parameters, according to the most recent studies on healthy subjects, the ground truth was chosen as $0.48 \times 10^{-3}\ mm^2/s$ for D, 13% for f and $18 \times 10^{-3}\ mm^2/s$ for D^*; 2) with respect to the data acquisition parameters, the set of b-values used in vivo, i.e., 0,50,100,150,400,800,1000 s/mm^2, was employed. Rician noise was added to the noise-free IVIM signal to generate data of different SNR (10, 20, 50 and 100), through the adjustment of the noise variance. For each SNR value, 10000 Monte Carlo (MC) trials were performed. The relative error of parameter $\theta_i \in \{f, D, D^*\}, \forall i \in \{1, 2, 3\}$ computed as $\frac{|\theta_i - \hat{\theta_i}|}{\theta_i}$ where $\hat{\theta}_i$ is the estimated value, was considered in order to evaluate and compare the performances of the five algorithms.

The second experiment was designed to investigate the algorithm performances for a range of tissue IVIM parameters, as it may occur in the presence of pathologies. A numerical phantom composed of 16 square regions was designed, with each region consisting of 6×6 pixels. All 36 pixels of each region were characterized by the same ground truth value of the IVIM parameters; for each pixel an MC trial was conducted. Since the diffusion coefficient is typically well estimated, it was decided to vary only the IVIM perfusion-related parameters f and D^* and the value of D was fixed to $0.48 \times 10^{-3}\ mm^2/s$. Sixteen combinations of IVIM parameters were obtained from the following two sets: $f \in \{5, 10, 15, 20\}(\%)$ and $D^* \in \{6, 12, 18, 24\}(\times 10^{-3}\ mm^2/s)$. Simulations for this numerical phantom were performed with an SNR of 20.

2.4 In vivo data analysis

The estimation of the IVIM parameters based on voxel-by-voxel analysis was performed on lumbar vertebrae (L1 to L5) of volunteers with the five different algorithms and parametric maps of D, f and D^* were generated.

2.5 Statistical analysis

A statistical analysis of the values of the IVIM parameters estimated from the data acquired in vivo was carried out. The IVIM parameters

obtained by each algorithm were compared using a one-way repeated-measures analysis of variance (ANOVA) followed by Bonferroni's multiple comparison test. A threshold of 5% was chosen for statistical significance. Statistical analyses were performed with GraphPad Prism (GraphPad, La Jolla, CA, USA).

2.6 Time cost

The time cost of each algorithm for the IVIM quantification of a single voxel was determined, by averaging the time cost over 10^4 repetitions. Calculations were conducted with MATLAB (R2020b) on a personal computer (Intel CPU, four cores, main frequency 2.4 GHz).

3 Results

RESOLVE MR images of the spine of a young healthy volunteer are shown in Fig. 1. Given the relatively long TE of 58 ms, the MR image at $b = 0\ s/mm^2$ (Fig. 1a) yields a T2-weighted image, with a high signal intensity from the intervertebral disks and cerebrospinal fluid (CSF), for instance. In the diffusion-weighted MR images (Fig. 1b and 1c), in particular at $b = 1000\ s/mm^2$, vertebral bone marrow appears hyper-intense compared to surrounding tissues, indicating a small diffusion coefficient of water molecules in bone marrow. For better visualization, the image contrast was adjusted separately on each image.

Overall, a good image quality and SNR can be observed on these diffusion-weighted images and no major artifacts are noticeable on the L1-L5 vertebrae. The SNR calculated using the repeated acquisition method was equal to 16.4 ± 3.1, when averaged over the lumbar vertebrae of five (out the six) volunteers. The SNR value of each vertebra is provided in Supplementary Materials (see Table S1). Furthermore, an example of the signal vs b-values plot is also shown in Supplementary Materials (see Figure S1).

Fig. 2 illustrates the results of the first simulation study for the estimation of the IVIM parameters D, f and D^* by the five algorithms. Four values of SNR (10, 20, 50, 100) are considered. The ground-truth value of D, f and D^* is indicated by the horizontal blue line on each graph. The first observation is that the Bayesian-based

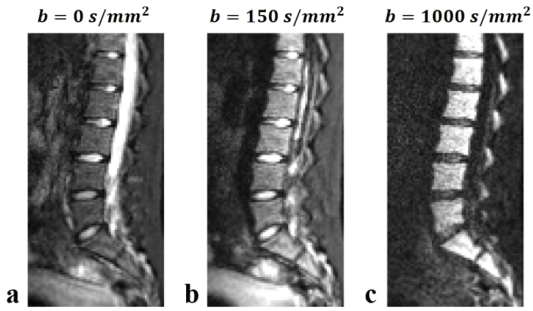

Fig. 1: Sagittal MR images of the spine of a young healthy volunteer, acquired with the RESOLVE MRI sequence. At $b = 1000\ s/mm^2$, the high signal intensity of vertebral bone marrow is indicative of a small diffusion coefficient of water molecules in vertebrae. For better visualization, a zoom-in of the lumbar vertebrae is displayed

approach yielded a more accurate and precise estimation of IVIM parameters, when compared to the four LSQ-based algorithms, for all values of SNR. Overall, at the SNR $\geq$ 20 the Bayesian approach provided a good estimation of D, f and D^*. With respect to the four deterministic algorithms, the following general considerations apply: i) at the SNR of 10 (black box-plot) the estimation of D, f and D^* suffered from a very poor precision; ii) at the SNR of 20 (red box-plot), the diffusion coefficient D was well estimated by all four algorithms; iii) for a good quantification of the perfusion fraction, an SNR between 20 and 50 was necessary. Finally, it can be noted that the estimation of D^* remained challenging even at high values of SNR. The relative error in the estimation of D, f and D^*, obtained by the same simulations of Fig. 2, is shown in Fig. 3.

The results of the second simulation study are shown in Fig. 4. The numerical phantom is illustrated with different colorbars for D (Fig. 4a), f (Fig. 4b) and D^* (Fig. 4c). Each of the 16 square regions is characterized by a unique combination of D, f and D^*. For instance, the ground truth values of the top-right square region are: $[D,f,D^*]=[0.48, 5, 24](10^{-3}\ mm^2/s$, $\%$, $10^{-3}\ mm^2/s)$. Overall, for all 16 combinations of f and D^* the Bayesian approach yielded a better estimation of the IVIM parameters compared to the deterministic algorithms. To be more specific, it could be easily observed from Fig. 4 that

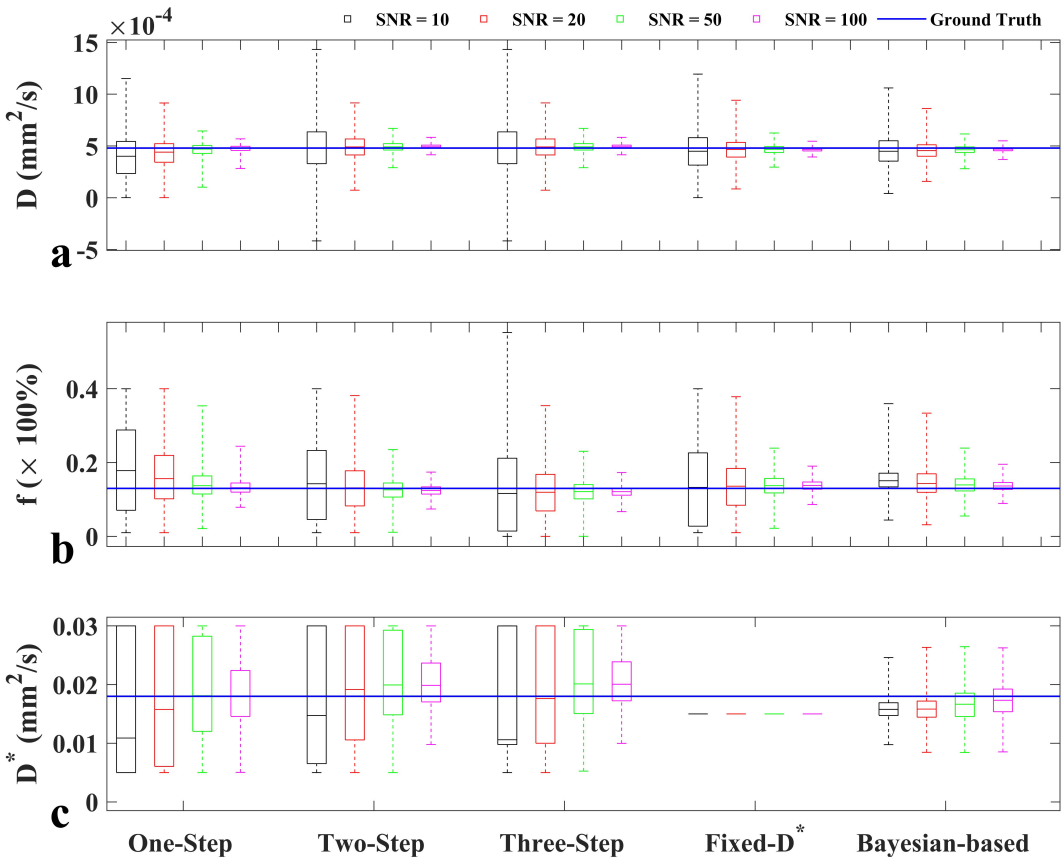

Fig. 2: Quantification of the IVIM parameters D (a), f (b) and D^* (c) with five algorithms (One-Step, Two-Step, Three-Step, Fixed-D^* and Bayesian-based). Each box plot includes simulated data from 10000 Monte Carlo trials. The blue line in each plot indicates the ground truth value for each parameter: $0.48 \times 10^{-3}\ mm^2/s$ for D, 13% for f and $18 \times 10^{-3}\ mm^2/s$ for D^*. Different colors illustrate a different SNR (black-box: SNR = 10; red-box: SNR = 20; etc.)

the maps provided by Bayesian-based algorithm, especially for f and D^*, were much smoother than maps from LSQ-based ones. Thus, the Bayesian-based algorithm outperforms deterministic ones since it provides estimated parameters not only closer to the ground truth but also of lower variability.

The parametric maps of D, f and D^* in vertebral bone marrow of one volunteer are illustrated in Fig. 5. In Fig. 5a, the MR image at $b = 0\ s/mm^2$ and the MR image at $b = 1000\ s/mm^2$ with the segmentation of the lumbar vertebrae are shown. For clarity, three different colorbars are employed for the parametric maps of D (Fig. 5b), f (Fig. 5c) and D^* (Fig. 5d). It can be noted that i) all five algorithms yielded parametric maps of similar quality for the diffusion coefficient D and ii) the Bayesian approach provided improved precision compared to the deterministic algorithms.

The values of D, f and D^* estimated for each vertebra in each volunteer (V1-V6) are illustrated in Fig. 6. Visual inspection of the data reveal that the values of f estimated by the One-Step algorithm (pink marker) are close to those estimated by Bayesian algorithm (blue marker, Fig. 6b). A

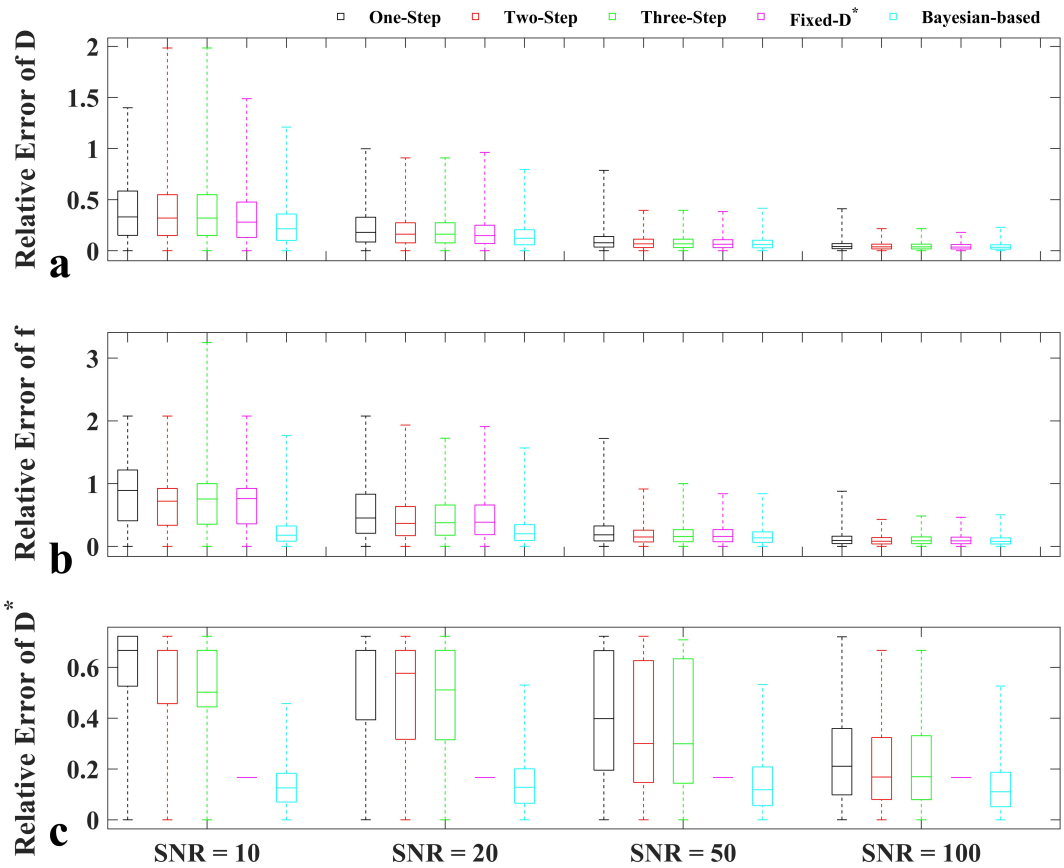

Fig. 3: The relative error for the IVIM parameters D (a), f (b) and D^* (c) at different values of signal-to-noise-ratio (SNR), estimated by the five algorithms (One-Step, Two-Step, Three-Step, Fixed-D^* and Bayesian-based)

statistical analysis was performed on all data: a total of 30 vertebrae ($n = 30$), with each vertebra evaluated using five algorithms. The following results were observed: for the diffusion coefficient D, in 22 out of 30 cases the ANOVA test with Bonferroni's post-test did not show a statistically significant difference between the values estimated by the One-Step and those estimated by Bayesian algorithm. On the contrary, for all other paired comparisons (One-Step vs Two-Step, One-Step vs Three-Step and so on) a statistically significant difference was observed in most vertebrae.

The statistical analysis of the perfusion fraction f yielded results similar to those for the diffusion coefficient D: i) 27 out of 30 cases did not show a statistically significant difference between the One-Step and Bayesian algorithm; this finding can be also easily confirmed by visual inspection of Fig. 6b and ii) for all other paired comparisons a statistically significant difference was observed in most vertebrae. The statistical results of all possible comparisons are provided in Supplementary Materials (Table S2). In Table 2, the average values of the IVIM parameters in the lumbar vertebra L1 over all volunteers are displayed. It is of interest to note that the average values of D and f estimated by the One-Step and Bayesian-based algorithms were close to each other. Furthermore, it can be noted that a lower value of D and a higher value of f were estimated by One-Step

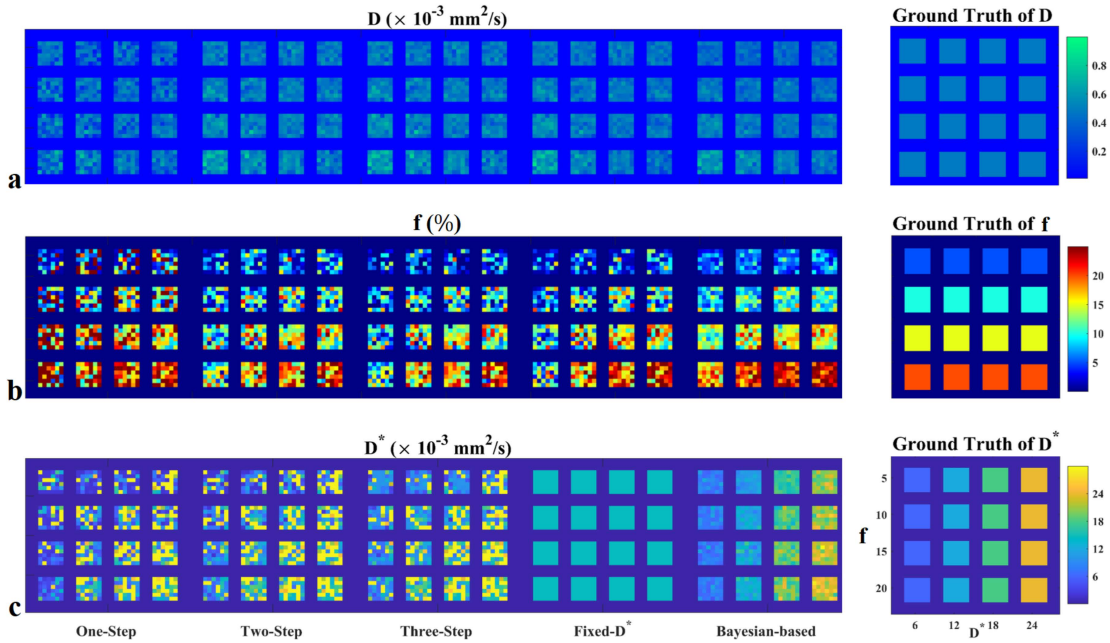

Fig. 4: Numerical phantom for estimation the IVIM parameters D (a), f (b) and D^* (c), using the five algorithms (One-Step, Two-Step, Three-Step, Fixed-D^* and Bayesian-based). Each of the 16 square regions is characterized by a unique combination of D, f and D^*, with the numerical values indicated for clarity only on the right panel of subfigure (c). In all cases, the value of D was fixed to 0.48×10^{-3} mm^2/s and the SNR was equal to 20. For all 16 combinations of f and D^* the Bayesian approach yielded a better estimation of the IVIM parameters when compared to the deterministic algorithms

Table 2: Example of IVIM quantification in the lumbar vertebra L1 using the five algorithms. The mean values of D, f and D^* are obtained from the parametric maps over all six volunteers

Algorithm	D $(\times 10^{-3}$ $mm^2/sec)$	f (%)	D^* $(\times 10^{-3}$ $mm^2/sec)$
One-Step	0.44	13.2	13.4
Two-Step	0.49	10.9	15.5
Three-Step	0.49	9.5	15.8
Fixed-D^*	0.47	10.4	15.0
Bayesian-based	0.44	13.8	15.1

and Bayesian-based algorithms when compared to the segmented approaches Two-Step, Three-Step, Fixed-D^*. The full results of each lumbar vertebra and each volunteer are provided in Supplementary Materials (Table S3 and Table S4). The parameters' estimates of D, f and D^* in volunteer 1 (lumbar vertebra L1) in two repeated measurements are shown in Table 3. Furthermore, a repeatability analysis (the coefficient of variation of D, f and D^*) calculated from two repeated measurements on 5 volunteers is provided in Supplementary Materials (Table S5 and Table S6).

The time cost of each algorithm for the IVIM quantification of a single voxel was determined; the results (in msec) were the following: 19.1, 19.0, 18.9, 18.4 and 2266 for the One-Step, Two-Step, Three-Step, Fixed-D^* and Bayesian-based algorithm, respectively. Thus, the four deterministic algorithms were much faster than the Bayesian-based one.

Table 3: The parameters' estimates of volunteer 1 (lumbar vertebra L1) in two repeated measurements

(Measurement 1)	D ($\times 10^{-3}$ mm^2/sec)	f (%)	D^* ($\times 10^{-3}$ mm^2/sec)
One-Step	0.42 ± 0.14	14.4 ± 11.4	14.0 ± 10.6
Two-Step	0.49 ± 0.13	11.7 ± 10.1	16.3 ± 10.6
Three-Step	0.49 ± 0.13	10.1 ± 10.4	16.5 ± 9.1
Fixed-D^*	0.46 ± 0.13	11.6 ± 10.6	15.0 ± 0.0
Bayesian-based	0.43 ± 0.14	14.6 ± 4.3	15.4 ± 2.6
(Measurement 2)			
One-Step	0.42 ± 0.15	13.1 ± 10.6	16.5 ± 11.3
Two-Step	0.47 ± 0.14	11.3 ± 9.5	18.0 ± 10.6
Three-Step	0.47 ± 0.14	10.6 ± 10.0	18.4 ± 9.4
Fixed-D^*	0.44 ± 0.13	11.7 ± 10.4	15.0 ± 0.0
Bayesian-based	0.42 ± 0.16	13.6 ± 4.8	15.5 ± 2.6

A comparison between the relative error of D, f and D^* obtained by the deterministic algorithms and the Bayesian-based one is provided in Supplementary Materials (Figure S2).

4 Discussion

In the current study, we have investigated five algorithms for the quantification of the IVIM parameters in vertebral bone marrow of young healthy volunteers. VBM-IVIM data were acquired using the RESOLVE sequence. Overall, numerical simulations and analysis of in vivo data indicated that the Bayesian method provided a better estimation of D, f and D^* than the deterministic algorithms. The advantage of the Bayesian methods over deterministic algorithms is particularly evident when observing the parametric maps of the VBM-IVIM perfusion fraction. Disadvantages of the Bayesian approach include the computational burden, the need of coding/implementation of the algorithm, whereas the deterministic algorithms are fast and readily available as in common programming environments. Among the deterministic algorithms, the One-Step is to prefer in the case of a good SNR - as in the case of ROI analysis for instance; on the other hand, the segmented approaches are of interest for analysis of data with limited SNR.

While there have been advances in VBM-IVIM data acquisition in recent years, little attention has been paid to data analysis methods for improving the quantification of VBM-IVIM parameters. In previous MRI IVIM studies, different data-fitting approaches for the estimation of IVIM parameters have been investigated for organs/tissues [14–19] other than bone marrow; furthermore, only a few of them have investigated the Bayesian method. The need of a dedicated study for VBM-IVIM stems from the fact that the performances of different algorithms depend on parameters that are related 1) to the organ/tissue under investigation and 2) to the specific experimental set-up. These parameters include i) tissue characteristics – in other words, the values of D, f and D^*; and ii) the image data quality – and in particular the SNR, which also depends on whether the analysis is performed on global ROIs or on a voxel-by-voxel basis to generate parametric maps.

With respect to tissue characteristics, vertebral bone marrow is a unique tissue, with a high lipid content. The adipocytes represent impermeable barriers to the diffusion motion of water molecules; as a result, the diffusion of water is highly hindered, resulting in a diffusion coefficient smaller ($0.2-0.6\times 10^{-3}$ mm^2/s) than that of most tissues [12]. In addition, the value of D^* is also smaller than that of other tissues [3, 13, 15, 34]. With respect to the overall image data quality, substantial improvements have been achieved by using the RESOLVE sequence combined with novel fat suppression techniques, compared to single shot EPI with STIR fat suppression. In the current study, SNR measurements were also performed – since the numerical value of SNR is a critical parameter, necessary when comparing the performances of different algorithms. Despite the fact that SNR measurements with the dual acquisition approach are simple to perform, to the best

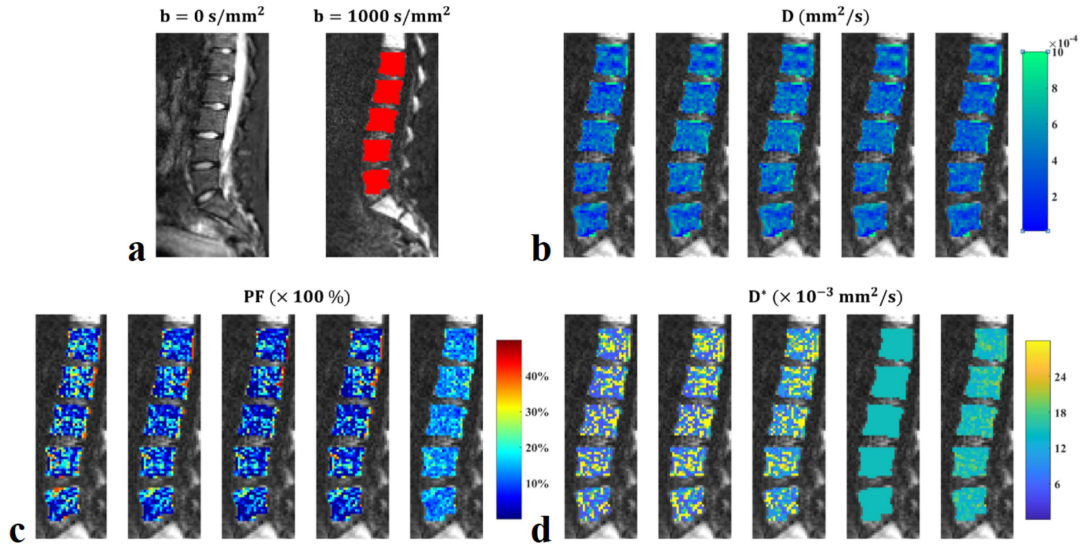

Fig. 5: MR images at $b = 0\ s/mm^2$ and $b = 1000\ s/mm^2$, with the segmentation of the lumbar vertebrae (a) and in vivo estimation the IVIM parameters D (b), f (c) and D^* (d), using the five algorithms. From left to right, the order of the five algorithms is the following: One-Step, Two-Step, Three-Step, Fixed-D^* and Bayesian-based. All five algorithms provide parametric maps of similar quality for the diffusion coefficient D. With respect to f and D^*, the precision of the Bayesian approach is superior to that of the deterministic algorithms

of our knowledge there have been no data in the literature providing SNR values for a VBM-IVIM protocol; we suggest that it might be useful, when setting up clinical VBM-IVIM studies, to determine on one or two participants the value of SNR for the specific experimental protocol.

4.1 Data acquisition

The typical data acquisition approach of VBM-IVIM consists of a spin-echo diffusion-preparation module followed by a single-shot EPI readout. As previously said, the RESOLVE sequence has been applied to VBM-IVIM, with the advantage of providing MR images with an overall improved quality compared to the single-shot EPI; however, the disadvantage of RESOLVE is a longer acquisition time. In the current study the RESOLVE protocol as proposed by Lasbleiz et al. [13] was applied, with an acquisition time of 4 minutes 40 seconds; as such, it could be an attractive alternative to single-shot EPI, since an MR sequence that lasts less than five minutes could be still acceptable in standard clinical examinations.

4.2 Comparison between simulation results and in vivo results

It is noteworthy the agreement in the IVIM parameter estimation by different algorithms between simulated results and in vivo results. In particular, two main findings are of interest. First, in the simulations a slight overestimation of D, was observed for the Two-Step and Three-Step algorithm, compared to i) the One-Step and Bayesian algorithm and ii) the ground truth values, as shown in Fig. 2. A similar behavior was observed in the results in vivo, that is, a slight overestimation of D for the Two-Step and Three-Step algorithm, compared to the One-Step and Bayesian algorithm, as illustrated in Fig. 6 and Table 2. Clearly, for the results in vivo there are no ground truth values for comparison. The second finding is related to the quantification of the perfusion fraction by the five algorithms. When compared to the ground truth, an underestimation of f for the Two-Step and Three-Step algorithm and an overestimation of f the One-Step and Bayesian algorithm is noteworthy. The same result

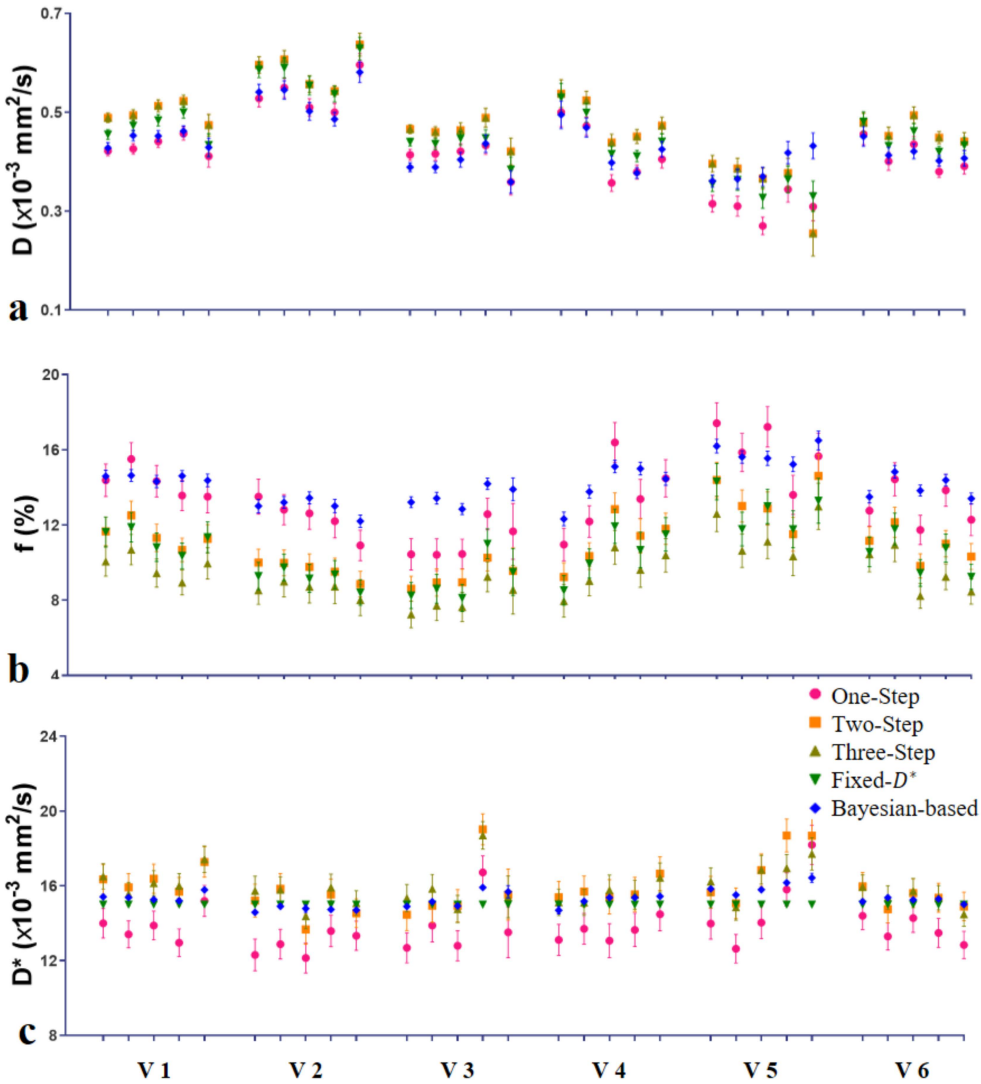

Fig. 6: The full results of the VBM-IVIM quantification in vivo, for six volunteers (V1-V6) and five lumbar vertebrae (L1-L5) using the five algorithms (One-Step, Two-Step, Three-Step, Fixed-D^* and Bayesian-based). The average values and the standard error of D, f and D^* are illustrated. In general, i) the One-step (pink marker) and Bayesian method (blue marker) provided similar values of D, f and ii) the One-step method displayed the highest standard error, when compared to all other methods

is obtained in vivo – this time when comparing the algorithms among themselves, since no ground truth is available. Overall, the Bayesian algorithm showed better performances when compared the deterministic algorithms. In general, in previous studies, it has been shown that the Bayesian-based algorithm outperforms LSQ-based ones. This is the case for instance in upper abdominal organs of healthy volunteers [15], in cancerous pancreas [17], and in cancerous lesions of breast [19]. In other studies, the Bayesian-based algorithm shows no advantage [18] over LSQ-based approaches. This apparent inconsistency of the results in the literature might be explained by the fact that the data analysis was performed on

different data (characterized by different SNR values); as a matter of fact, with respect to data of higher SNR, the Bayesian-based algorihtm has a limited added value, as it can be observed in the Fig. 2 and Fig. 3 (especially for SNR = 50 and SNR = 100). In contrast to other organs, IVIM of bone marrow suffers from low SNR due to lower water content and shorter transverse relaxation time [35]. In this case, the Bayesian-based algorithm is an attractive alternative to LSQ-based ones. However, despite the very good performance of Bayesian algorithm, its use is to some extent limited in practice. This is generally due to i) its relatively high numerical complexity; ii) the lack of available implementation in commonly used programming environments in contrast to deterministic algorithms; iii) its sensitivity to the choice of the parameters' prior distributions and the employed posterior central tendency measures [29]. Note that the bounded Gaussian prior distribution and the mean measure of posterior central tendency were used in the current study.

There are a number of limitations to this study. Only six volunteers were examined. Further studies are necessary to investigate the impact of the different algorithms on the quantification of IVIM parameters in a patient population. Furthermore, only young volunteers were included in the current study; the quantification of VBM-IVIM parameters when using the same protocol of the current study might suffer from a lower SNR when examining older volunteers, who typically have a higher lipid fraction in vertebral bone marrow.

In addition, a digital phantom with uniform ground truth was employed; the potential over smoothing of a heterogeneous ground truth was not investigated.

In conclusion, the impact of five different algorithms for quantification of IVIM parameters in vertebral bone marrow was investigated. The Bayesian approach provided the best estimation, as shown by simulations and in vivo parametric maps.

Author contributions. All authors contributed to the conception and design of the study. The acquisition of data was performed by LM. The data analysis was performed by JL and GG. All authors contributed to the interpretation and discussion of the results. The first draft of the manuscript was written by JL and GG. All authors read and approved the final manuscript. All authors agree to be accountable for all aspects of this study in ensuring that questions related to any part of the work can be properly investigated and resolved.

Declarations

Conflict of interest The authors declare that they have no conflict of interest.

Ethics approval All experiments were conducted in accordance with the procedures approved by the local Institutional Review Board. Written informed consent was signed by each volunteer before the measurements.

References

[1] Bihan, D.L., Breton, E., Lallemand, D., Grenier, P., Cabanis, E., Laval-Jeantet, M.: Mr imaging of intravoxel incoherent motions: application to diffusion and perfusion in neurologic disorders. Radiology **161**, 401–407 (1986). https://doi.org/10.1148/radiology.161.2.3763909

[2] Yeung, D.K.W., Wong, S.Y.S., Griffith, J.F., Lau, E.M.C.: Bone marrow diffusion in osteoporosis: Evaluation with quantitative mr diffusion imaging. Journal of Magnetic Resonance Imaging **19**, 222–228 (2004). https://doi.org/10.1002/jmri.10453

[3] Marchand, A.J., Hitti, E., Monge, F., Saint-Jalmes, H., Guillin, R., Duvauferrier, R., Gambarota, G.: Mri quantification of diffusion and perfusion in bone marrow by intravoxel incoherent motion (ivim) and non-negative least square (nnls) analysis. Magnetic Resonance Imaging **32**, 1091–1096 (2014). https://doi.org/10.1016/j.mri.2014.07.009

[4] Bourillon, C., Rahmouni, A., Lin, C., Belhadj, K., Beaussart, P., Vignaud, A., Zerbib, P., Pigneur, F., Cuenod, C.-A., Bessalem, H., Cavet, M., Boutekadjirt, A., Haioun, C., Luciani, A.: Intravoxel incoherent motion diffusion-weighted imaging of multiple myeloma lesions: Correlation with whole-body dynamic contrast agent–enhanced mr

imaging. Radiology **277**, 773–783 (2015). https://doi.org/10.1148/radiol.2015141728

[5] Baik, J.S., Jung, J.-Y., Jee, W.-H., Chun, C.-W., Kim, S.K., Shin, S.H., Chung, Y.G., Jung, C.-K., Kannengiesser, S., Sohn, Y.: Differentiation of focal indeterminate marrow abnormalities with multiparametric mri. Journal of magnetic resonance imaging : JMRI **46**, 49–60 (2017). https://doi.org/10.1002/jmri.25536

[6] Lee, E.Y.P., Perucho, J.A.U., Vardhanabhuti, V., He, J., Siu, S.W.K., Ngu, S.F., Mayr, N.A., Yuh, W.T.C., Chan, Q., Khong, P.-L.: Intravoxel incoherent motion mri assessment of chemoradiation-induced pelvic bone marrow changes in cervical cancer and correlation with hematological toxicity. Journal of Magnetic Resonance Imaging **46**, 1491–1498 (2017). https://doi.org/10.1002/jmri.25680

[7] Niu, J., Li, W., Wang, H., Wu, W., Gong, T., Huang, N., Wang, J., Qi, Y.: Intravoxel incoherent motion diffusion-weighted imaging of bone marrow in patients with acute myeloid leukemia: a pilot study of prognostic value. Journal of Magnetic Resonance Imaging **46**, 476–482 (2017). https://doi.org/10.1002/jmri.25600

[8] Park, S., Kwack, K.-S., Chung, N.-S., Hwang, J., Lee, H.Y., Kim, J.H.: Intravoxel incoherent motion diffusion-weighted magnetic resonance imaging of focal vertebral bone marrow lesions: initial experience of the differentiation of nodular hyperplastic hematopoietic bone marrow from malignant lesions. Skeletal Radiology **46**, 675–683 (2017). https://doi.org/10.1007/s00256-017-2603-z

[9] Yoon, M.A., Hong, S.-J., Lee, C.H., Kang, C.H., Ahn, K.-S., Kim, B.H.: Intravoxel incoherent motion (ivim) analysis of vertebral bone marrow changes after radiation exposure from diagnostic imaging and interventional procedures. Acta Radiologica **58**, 1260–1268 (2017). https://doi.org/10.1177/0284185116688380

[10] Li, J., Zheng, R., Niu, J., Song, X., Wu, W., Fan, R., Gong, T.: Correlation of intravoxel incoherent motion parameters and histological characteristics from infiltrated marrow in patients with acute leukemia. Journal of Magnetic Resonance Imaging **51**, 1720–1726 (2020). https://doi.org/10.1002/jmri.26999

[11] Chen, Y., Yu, Q., Tegola, L.L., Mei, Y., Chen, J., Huang, W., Zhang, X., Guglielmi, G.: Intravoxel incoherent motion mr imaging for differentiating malignant lesions in spine: A pilot study. European Journal of Radiology **120**, 108672 (2019). https://doi.org/10.1016/j.ejrad.2019.108672

[12] Dietrich, O., Geith, T., Reiser, M.F., Baur-Melnyk, A.: Diffusion imaging of the vertebral bone marrow. NMR in Biomedicine **30**, 3333 (2017). https://doi.org/10.1002/nbm.3333

[13] Lasbleiz, J., Ster, C.L., Guillin, R., Saint-Jalmes, H., Gambarota, G.: Measurements of diffusion and perfusion in vertebral bone marrow using intravoxel incoherent motion (ivim) with multishot, readout-segmented (resolve) echo-planar imaging. Journal of Magnetic Resonance Imaging **49**, 768–776 (2019). https://doi.org/10.1002/jmri.26270

[14] Porter, D.A., Heidemann, R.M.: High resolution diffusion-weighted imaging using readout-segmented echo-planar imaging, parallel imaging and a two-dimensional navigator-based reacquisition. Magnetic Resonance in Medicine **62**, 468–475 (2009). https://doi.org/10.1002/mrm.22024

[15] Barbieri, S., Donati, O.F., Froehlich, J.M., Thoeny, H.C.: Impact of the calculation algorithm on biexponential fitting of diffusion-weighted mri in upper abdominal organs. Magnetic Resonance in Medicine **75**, 2175–2184 (2016). https://doi.org/10.1002/mrm.25765

[16] Heusch, P., Wittsack, H.-J., Pentang, G., Buchbender, C., Miese, F., Schek, J., Kröpil, P., Antoch, G., Lanzman, R.S.: Biexponential analysis of diffusion-weighted imaging: comparison of three different calculation methods in transplanted kidneys. Acta Radiologica **54**, 1210–1217 (2013). https://doi.org/10.1177/

0284185113491090

[17] Gurney-Champion, O.J., Klaassen, R., Froeling, M., Barbieri, S., Stoker, J., Engelbrecht, M.R.W., Wilmink, J.W., Besselink, M.G., Bel, A., van Laarhoven, H.W.M., Nederveen, A.J.: Comparison of six fit algorithms for the intra-voxel incoherent motion model of diffusion-weighted magnetic resonance imaging data of pancreatic cancer patients. PLOS ONE **13**, 0194590 (2018). https://doi.org/10.1371/journal.pone.0194590

[18] Jalnefjord, O., Andersson, M., Montelius, M., Starck, G., Elf, A.-K., Johanson, V., Svensson, J., Ljungberg, M.: Comparison of methods for estimation of the intravoxel incoherent motion (ivim) diffusion coefficient (d) and perfusion fraction (f). **31**, 715–723 (2018). https://doi.org/10.1007/s10334-018-0697-5

[19] Vidić, I., Jerome, N.P., Bathen, T.F., Goa, P.E., While, P.T.: Accuracy of breast cancer lesion classification using intravoxel incoherent motion diffusion-weighted imaging is improved by the inclusion of global or local prior knowledge with bayesian methods. Journal of Magnetic Resonance Imaging **50**, 1478–1488 (2019). https://doi.org/10.1002/jmri.26772

[20] Meeus, E.M., Novak, J., Withey, S.B., Zarinabad, N., Dehghani, H., Peet, A.C.: Evaluation of intravoxel incoherent motion fitting methods in low-perfused tissue. Journal of Magnetic Resonance Imaging **45**, 1325–1334 (2017). https://doi.org/10.1002/jmri.25411

[21] Neil, J.J., Bretthorst, G.L.: On the use of bayesian probability theory for analysis of exponential decay date: An example taken from intravoxel incoherent motion experiments. Magnetic Resonance in Medicine **29**, 642–647 (1993). https://doi.org/10.1002/mrm.1910290510

[22] Firbank, M.J., Coulthard, A., Harrison, R.M., Williams, E.D.: A comparison of two methods for measuring the signal to noise ratio on mr images. Physics in medicine and biology **44**, 261–4 (1999). https://doi.org/10.1088/0031-9155/44/12/403

[23] Ayyub, B.M., McCuen, R.H.: Trust-Region Methods. https://doi.org/10.1007/978-0-387-40065-5_4. http://link.springer.com/10.1007/978-0-387-40065-5_4

[24] Patel, J., Sigmund, E.E., Rusinek, H., Oei, M., Babb, J.S., Taouli, B.: Diagnosis of cirrhosis with intravoxel incoherent motion diffusion mri and dynamic contrast-enhanced mri alone and in combination: Preliminary experience. Journal of Magnetic Resonance Imaging **31**, 589–600 (2010). https://doi.org/10.1002/jmri.22081

[25] Pekar, J., Moonen, C.T.W., van Zijl, P.C.M.: On the precision of diffusion/perfusion imaging by gradient sensitization. Magnetic Resonance in Medicine **23**, 122–129 (1992). https://doi.org/10.1002/mrm.1910230113

[26] Lemke, A., Laun, F.B., Simon, D., Stieltjes, B., Schad, L.R.: An in vivo verification of the intravoxel incoherent motion effect in diffusion-weighted imaging of the abdomen. Magnetic Resonance in Medicine **64**, 1580–1585 (2010). https://doi.org/10.1002/mrm.22565

[27] Orton, M.R., Collins, D.J., Koh, D.-M., Leach, M.O.: Improved intravoxel incoherent motion analysis of diffusion weighted imaging by data driven bayesian modeling. Magnetic Resonance in Medicine **71**, 411–420 (2014). https://doi.org/10.1002/mrm.24649

[28] While, P.T.: A comparative simulation study of bayesian fitting approaches to intravoxel incoherent motion modeling in diffusion-weighted mri. Magnetic resonance in medicine **78**, 2373–2387 (2017). https://doi.org/10.1002/mrm.26598

[29] Gustafsson, O., Montelius, M., Starck, G., Ljungberg, M.: Impact of prior distributions and central tendency measures on bayesian intravoxel incoherent motion model fitting. Magnetic Resonance in Medicine **79**, 1674–1683 (2018). https://doi.org/10.1002/mrm.26783

[30] JEFFREYS, H.: The theory of probability. Nature **109**, 132–133 (1922). https://doi.org/10.1038/109132a0

[31] Bretthorst, G.L., Hutton, W.C., Garbow, J.R., Ackerman, J.J.H.: Exponential parameter estimation (in nmr) using bayesian probability theory. Concepts in Magnetic Resonance Part A: Bridging Education and Research **27**, 55–63 (2005). https://doi.org/10.1002/cmr.a.20043

[32] Neal, R.M.: Probabilistic Inference Using Markov Chain Monte Carlo Methods (1993)

[33] Lynch, S.M.: Modern Model Estimation Part 2: Metroplis–Hastings Sampling. https://doi.org/10.1007/978-0-387-71265-9_5. http://link.springer.com/10.1007/978-0-387-71265-9_5

[34] Gambarota, G., Hitti, E., Leporq, B., Saint-Jalmes, H., Beuf, O.: Eliminating the blood-flow confounding effect in intravoxel incoherent motion (ivim) using the non-negative least square analysis in liver. Magnetic Resonance in Medicine **77**, 310–317 (2017). https://doi.org/10.1002/mrm.26085

[35] Marage, L., Gambarota, G., Lasbleiz, J., Lederlin, M., Saint-Jalmes, H.: Confounding factors in multi-parametric q-mri protocol: A study of bone marrow biomarkers at 1.5 t. Magnetic Resonance Imaging **74**, 96–104 (2020)